A Single-Crystal ESR and Quantum Chemical Study of Electron-Capture Trialkylphosphine Sulfide and Selenide Radical Anions with a Three-Electron Bond

René A. J. Janssen,* Joost A. J. M. Kingma, and Henk M. Buck

Contribution from the Department of Organic Chemistry, Eindhoven University of Technology, Eindhoven, The Netherlands 5600 MB. *Received September 4, 1987*

Abstract: A low-temperature ESR study of electron-capture phosphoranyl radicals in X-irradiated single crystals of trialkylphosphine sulfides and selenides (R_3PX: X = S, Se; R = CH_3, C_2H_5, C_6H_{11}) is presented. The principal values and direction cosines of the **g** tensors and ^{31}P and ^{77}Se hyperfine coupling tensors are determined and correlated with the X-ray structure analysis of the parent compounds. All studied compounds reveal the formation of a $R_3\dot{P}X^-$ radical anion, with a three-electron P∴X bond in which the unpaired electron is nearly equally distributed over phosphorus and the substituent X. It is shown that the site symmetry of the radicals corresponds to the crystallographic point symmetry of the precursor molecules, resulting in pure trigonal (C_3) radicals for $(C_2H_5)_3\dot{P}X^-$ and C_s symmetry for $(CH_3)_3\dot{P}X^-$ and $(C_6H_{11})_3\dot{P}X^-$. Ab initio quantum chemical calculations (4-31G* SCF and CASSCF) on the model $H_3\dot{P}S^-$ predict that the three-electron bond is unstable and dissociates into PH_3 and $S^{\bullet-}$. The calculations do not reproduce the experimental couplings and the observed spin density distribution, but tend to localize the unpaired electron entirely on sulfur. The origin of this deficiency appears to be predominantly due to a poor description of the negative charge of the nonbonding electron pairs of the sulfur atom. Via the introduction of a positive charge in the vicinity of the sulfur atom, the theoretical spin density distribution can be brought in accordance with the experimental data. The use of quantum chemical calculations for the simulation of trapped radicals in the solid state is discussed.

I. Introduction

The nature of two-center, three-electron bonds (A∴B) has received much recent experimental[1-7] and theoretical[8-11] attention. The electronic structure of a three-electron bond is characterized by the combined effects of two bonding σ electrons and one antibonding, i.e., bond weakening σ^* electron. Three-electron bonds can be formed via the addition of an electron to an existing σ bond or via the inter- or intramolecular interaction of a single occupied molecular orbital (SOMO) and a free electron pair. It has been argued by various authors that a three-electron bond is significantly stabilized when the energy levels of the two molecular fragments involved in the bonding are (nearly) degenerate.[12-14] This is reflected in the relatively large number of symmetric three-electron bond radicals (A∴A) which are known experimentally.[15-20] Ab initio quantum chemical calculations on symmetric $\sigma^2\sigma^{*1}$ configurations invariable predict a stable three-electron bond.[11,21,22] On the other hand, asymmetric three-electron bonds (A–B) are far less familiar.[23,24] The asymmetry of the radical is likely to yield different energy levels for the overlapping SOMO and HOMO of the two constituents. Since stabilization due to three-electron (SOMO–HOMO) interaction falls off rapidly with increasing energy gap,[11] an asymmetric $\sigma^2\sigma^{*1}$ configuration is expected to be less stable.

In the present paper we report a low-temperature single-crystal ESR study of trialkylphosphine sulfide and selenide electron-capture radical anions ($R_3\dot{P}X^-$, X = S, Se; R = CH_3, C_2H_5, and C_6H_{11}), containing a three-electron bond (Figure 1).

A prerequisite for the formation of a P∴X$^-$ three-electron bond is that the substituent X and the PX bond can accommodate the extra electron appreciably better than the ligands R and the PR bonds. Hence, its formation is closely related to the parent P=X bond energy, because upon electron capture the antibonding component of the SOMO will tend to elongate the bond. Extensive experimental[25,26] and theoretical[27] studies have shown that the thiophosphoryl (PS) bond is weaker and contains less multiple bond character than does the phosphoryl (PO) bond. Typical dissociation energies of PS bonds are 443 versus 732 kJ mol^{-1} for the PO group.[28] The quantum chemical estimate of the bond order of the PS bond in H_3PS is 1.32, substantially less than the 1.58 bond order in H_3PO.[27] In consequence it can be expected that P∴X$^-$ three-electron bonds are more easily formed in phosphine sulfides and selenides than in the corresponding oxides.

From the ESR spectra of the $R_3\dot{P}X^-$ radicals and the observed ^{31}P and ^{77}Se hyperfine couplings it is concluded that the unpaired electron is approximately equally distributed over phosphorus and the chalcogen ligand. The orientation of the **g** tensor and the ^{31}P and ^{77}Se hyperfine coupling tensors is compared with the crystallographic bond directions of the parent compounds. It will be shown that the molecular symmetry adopted by the phosphoranyl

(1) Mohan, H.; Asmus, K.-D. *J. Am. Chem. Soc.* **1987**, *109*, 4745.
(2) Anklam, E.; Mohan, H.; Asmus, K.-D. *J. Chem. Soc., Chem. Commun.* **1987**, 629.
(3) Franzi, R.; Geoffroy, M.; Reddy, M. V. V. S.; Weber, J. *J. Phys. Chem.* **1987**, *91*, 3187.
(4) Janssen, R. A. J.; Sonnemans, M. H. W.; Buck, H. M. *J. Chem. Phys.* **1986**, *84*, 3694.
(5) Knight, L. B.; Earl, E.; Ligon, A. R.; Cobranchi, D. P. *J. Chem. Phys.* **1986**, *85*, 1228.
(6) Kirste, R.; Alder, R. W.; Sessions, R. B.; Bock, M.; Kurreck, H.; Nelsen, S. F. *J. Am. Chem. Soc.* **1985**, *107*, 2635.
(7) Hasegawa, A.; McConnachie, G. D. G.; Symons, M. C. R. *J. Chem. Soc., Faraday Trans.* **1984**, *80*, 1005.
(8) Nguyen, M. T.; Ha, T.-K. *Chem. Phys. Lett.* **1987**, *136*, 413.
(9) Glidewell, C. *J. Chem. Soc., Perkin Trans. 2* **1985**, 299.
(10) Glidewell, C. *J. Chem. Soc., Perkin Trans. 2* **1985**, 551.
(11) Clark, T. *J. Comput. Chem.* **1983**, *4*, 404.
(12) Anh, N. T.; Minot, C. *J. Am. Chem. Soc.* **1980**, *102*, 103.
(13) Baird, N. C. *J. Chem. Educ.* **1977**, *54*, 291.
(14) Göbl, M.; Bonifačić, M.; Asmus, K.-D. *J. Am. Chem. Soc.* **1984**, *106*, 5984.
(15) Alder, R. W.; Sessions, R. B. *J. Am. Chem. Soc.* **1979**, *101*, 3651.
(16) Gillbro, T.; Kerr, C. L. M.; Williams, F. *Mol. Phys.* **1974**, *28*, 1225.
(17) Hudson, R. L.; Williams, F. *J. Phys. Chem.* **1980**, *84*, 3483.
(18) Asmus, K.-D. *Acc. Chem. Res.* **1979**, *12*, 436.
(19) Nelsen, S. F.; Kessel, C. R.; Brien, D. J. *J. Am. Chem. Soc.* **1979**, *101*, 1874.
(20) Nishikida, K.; Williams, F. *Chem. Phys. Lett.* **1975**, *34*, 302.
(21) Bouma, W. J.; Radom, L. *J. Am. Chem. Soc.* **1985**, *107*, 345.
(22) Clark, T. *J. Comput. Chem.* **1982**, *3*, 112.
(23) Berclaz, T.; Geoffroy, M.; Lucken, E. A. C. *Chem. Phys. Lett.* **1975**, *36*, 677.
(24) Symons, M. C. R.; Petersen, R. L. *J. Chem. Soc., Faraday Trans. 2* **1979**, *75*, 210.
(25) Albright, T. A.; Freeman, W. J.; Schweizer, E. E. *J. Org. Chem.* **1975**, *40*, 3437.
(26) Carlson, R. R.; Meek, D. W. *Inorg. Chem.* **1974**, *13*, 1741.
(27) Schmidt, M. W.; Gordon, M. S. *J. Am. Chem. Soc.* **1985**, *107*, 1922.
(28) Huhee, J. E. *Inorganic Chemistry: Principles of Structure and Reactivity*; Harper and Row: New York, 1978.

0002-7863/88/1510-3018$01.50/0 © 1988 American Chemical Society

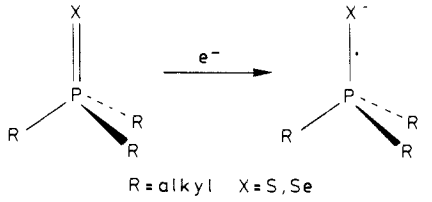

Figure 1. Formation of a R_3P-X^- configuration.

radicals corresponds to that of the single-crystal matrix resulting in pure C_3 (R = C_2H_5) or C_s (R = CH_3, C_6H_{11}) geometries. An attempt is made to describe the electronic structure and stability of these asymmetric three-electron bond radicals using quantum chemical methods. However, the employed ab initio SCF and CASSCF calculations do not predict stable geometries for isolated $R_3\dot{P}S^-$ radicals with a C_3 $\sigma^2\sigma^{*1}$ configuration. The calculations tend to move the unpaired electron entirely to the chalcogen ligand. Via the introduction of a positive charge in the vicinity of the negatively charged sulfur atom, shielding the lone-pair electrons, the theoretical spin density distribution can be brought into line with the experiments. This gives an indication of the limitation of ab initio quantum chemical calculations on isolated radical anions for the simulation of condensed-phase behavior.

II. Experimental Section

1. Synthesis. Trimethylphosphine sulfide (**1**) was obtained from the reaction of tetramethyldiphosphine disulfide and methyl iodide.[29] Triethylphosphine sulfide (**2**), tricyclohexylphosphine sulfide (**3**), trimethylphosphine selenide (**4**), triethylphosphine selenide (**5**), and tricyclohexylphosphine selenide (**6**) were synthesized from the corresponding phosphines and elemental sulfur or selenium.[30-32] Triphenylphosphine sulfide (**7**) and selenide (**8**) were commercial materials (Janssen Chimica). All compounds were characterized with ^1H and ^{31}P NMR and elemental analysis. Single crystals were prepared by slow evaporation or slow cooling of solutions of the desired compound in ethanol (**1**, **3**, **4**, **5**, **6**) or 1,4-dioxane (**2**, **8**).

2. Irradiation and ESR. Single crystals were mounted on a quartz rod and subsequently sealed in a quartz tube. The samples were X-irradiated at 77 K using unfiltered radiation from a Cu source for 6 h. ESR measurements were performed using a Bruker ER200D spectrometer, interfaced with a Bruker Aspect 3000 computer, operating with a X-band standard cavity. The single crystals were rotated perpendicular to the magnetic field with a single-axis goniometer in 10° steps. Temperature was controlled with the aid of a variable-temperature unit operating between 90 K and room temperature. ESR parameters were obtained from a second-order analysis of the spectra.

III. Results

1. Trimethylphosphine Sulfide (1). Trimethylphosphine sulfide (**1**) crystallizes in the monoclinic space group $P2_1/m$ with unit cell parameters a = 6.266 Å, b = 7.588 Å, c = 6.642 Å, and β = 90.36°.[33] Although the reported X-ray structure analysis is incomplete, the results suggest a small distortion of the molecules from C_{3v} to C_s symmetry. One SPC angle is slightly larger than the other two.

The ESR spectrum obtained at 105 K of a X-irradiated single crystal of **1** (Figure 2a) shows a ^{31}P doublet which can be attributed to the trimethylphosphine sulfide radical anion (**1a**). The high- and low-field transitions are broadened by a poorly resolved ^1H hyperfine coupling. From some orientations of the single crystal with respect to the magnetic field this coupling can be determined to be approximately 0.4–0.5 mT. Since the unit cell angle β is very close to 90° the three crystallographic axes were used as ESR reference axes. A complete single-crystal analysis of **1a** was obtained from rotation of the crystal in the *ab*, *ac*, and *bc* planes. It was found that the principal hyperfine tensor and the **g** tensor share the same principal axes, and also coincide with the crystallographic axes (Table I).

Table I. **g** and Hyperfine Coupling (MHz) Tensors for **1a** and **1b**

radical	temp (K)	total tensor		direction cosines *a*	*b*	*c*
1a	105	g	2.003	1	0	0
			2.010	0	1	0
			2.004	0	0	1
		^{31}P	2021	1	0	0
			1647	0	1	0
			1660	0	0	1
		^1H	~13	nearly isotropic		
1b	240	g	2.018	1	0	0
			2.012	0	1	0
			2.010	0	0	1
		^{31}P	771	1	0	0
			979	0	1	0
			1001	0	0	1
		^1H	~13	nearly isotropic		

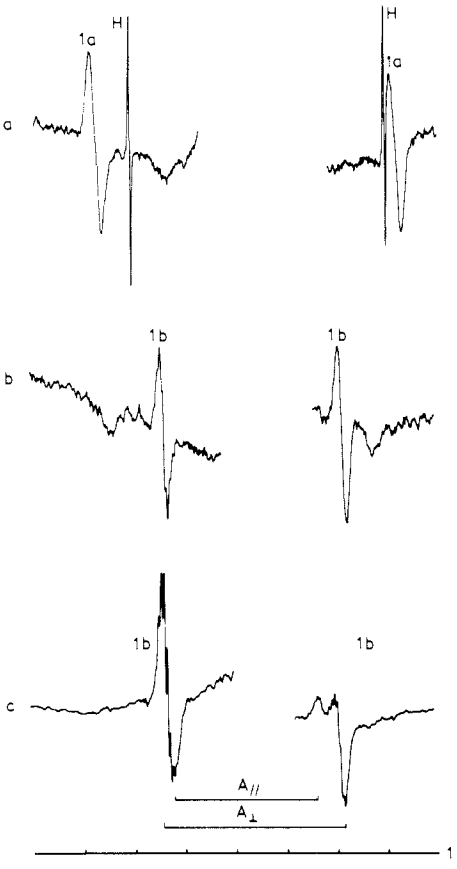

Figure 2. ESR spectra of X-irradiated $(CH_3)_3PS$ (**1**): (a) single-crystal ESR spectrum of **1a** at 105 K, magnetic field parallel to the *c* axis (lines marked H result from trapped hydrogen atoms); (b) single-crystal spectrum of **1b** at 240 K, magnetic field parallel to the *c* axis; (c) powder spectrum of **1b** at 200 K.

Upon raising the temperature, the intensity of the signals assigned to **1a** decreases and the radical is irreversibly lost at 180 K. Concurrently with the loss of **1a** a new phosphorus doublet **1b** with a smaller ^{31}P coupling is detected (Figure 2b). This newly formed radical remains in the single crystal for several hours, even at room temperature. The principal hyperfine couplings and *g* values of **1b** are directed along the three crystallographic axes (Table I), as for **1a**. Their magnitudes show, however, a very anomalous behavior because $A_\perp$ (=990 MHz) > $A_\parallel$ (=772 MHz) indicating an opposite sign for A^{iso} and B. Furthermore, all three *g* values deviate from the free-electron value. The powder spectrum of **1b** (Figure 2c) is in accordance with the single-crystal analysis and shows the expected pattern for a radical exhibiting $A_\parallel < A_\perp$ and $g_\parallel > g_\perp$. Radical **1b** exhibits additional ^1H splitting of approximately 0.5 mT.

(29) Tsvetkov, E. N.; Chepaikina, T. A.; Kabachnik, M. I. *Izv. Akad. Nauk SSSR, Ser. Khim.* **1979**, 426.
(30) Issleib, K.; Brach, A. *Z. Anorg. Allg. Chem.* **1954**, *277*, 258.
(31) Renshaw, R. R.; Bell, K. F. *J. Am. Chem. Soc.* **1921**, *43*, 916.
(32) Zingaro, R. A.; McGlothlin, R. E. *J. Org. Chem.* **1961**, *26*, 5205.
(33) Eller, P. G.; Corfield, P. W. R. *Chem. Commun.* **1971**, 105.

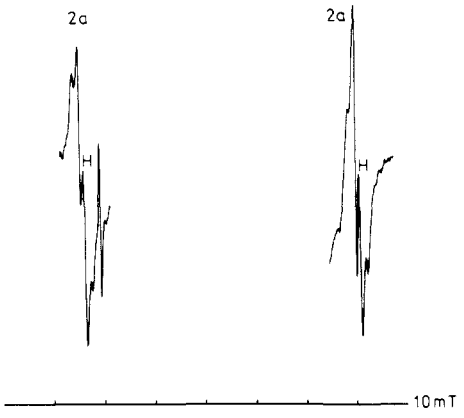

Figure 3. Single-crystal ESR spectrum of radical **2a** at 105 K. Lines marked H result from hydrogen atoms; magnetic field parallel to *c* axis.

Table II. g and Hyperfine Coupling (MHz) Tensors for **2a**

radical	temp (K)	total tensor		direction cosines *a*	*a*	*c*
2a	105	g	2.006	1	0	0
			2.006	0	1	0
			2.002	0	0	1
		^{31}P	1517	1	0	0
			1517	0	1	0
			1943	0	0	1
		^{1}H	~34	nearly isotropic		

The fact that the same axes system diagonalizes both the ^{31}P hyperfine tensor and the **g** tensor for **1a** as well as **1b**, and the observation that the ^{31}P hyperfine tensors are essentially axially symmetric, indicates an overall C_{3v} symmetry for the two radicals. Since the directions of the parallel hyperfine couplings also coincide with the *a* axis, the *a* axis must be the direction of the PS bond of the precursor molecule. This result is in accordance with the crystal structure analysis of trimethylphosphine selenide (section 3.4) which is isomorphous with that of the present compound.[34] The **g** tensor of **1a** dose not possess a C_{3v} symmetry. The principal value in the *b* direction is clearly different from those in the *ac* plane.

2. Triethylphosphine Sulfide (2). Triethylphosphine sulfide (**2**) crystallizes as long needles in the hexagonal space group $P6_3mc$. The cell dimensions are a = 8.98 Å and c = 6.32 Å.[35] The PS bond of the molecules is aligned along the *c* axis which is parallel to the needle axis. The molecules possess a staggered conformation of the ethyl groups. One of the CH_2 hydrogen atoms is in a trans location with respect to the PS bond. The methyl groups and the remaining hydrogen atom are in the gauche positions. The molecules possess a C_3 symmetry.

X irradiation of a single crystal of **2** at 77 K generates an electron-capture phosphoranyl radical **2a**. The ESR spectrum of **2a** (Figure 3) clearly shows a large ^{31}P doublet with an additional splitting due to three equivalent ^{1}H nuclei. This splitting of 1.2 mT is essentially isotropic.

For all orientations of the crystal with the *c* axis perpendicular to the magnetic field, identical spectra, giving $A_\perp$ and $g_\perp$, are observed. Rotation of the single crystal in the *ac* plane reveals the parallel values of the **g** and ^{31}P hyperfine coupling tensors (Table II). Both tensors are completely axially symmetric. From this observation it can be concluded that the irradiation process does not lead to any detectable distortion from C_3 symmetry for **2a**. The extra hyperfine splitting arises most likely from the three trans oriented ^{1}H nuclei. Radical **2a** is irreversibly lost from the ESR spectrum at 170 K. No new species could be detected.

3. Tricyclohexylphosphine Sulfide (3). Crystals of tricyclohexylphosphine sulfide (**3**) are orthorhombic with a = 10.906 Å, b = 15.836 Å, and c = 10.362 Å.[36] The reported crystal structure parameters refer to the centrosymmetric space group *Pnma*. The four molecules in the unit cell lie on a mirror plane which is parallel to the *ac* plane. The PS bond directions are pairwise aligned, resulting in two different orientations, which are inclined by an angle of 15.8°. Recrystallization gives plate-like crystals (*b* axis perpendicular to the plate face).

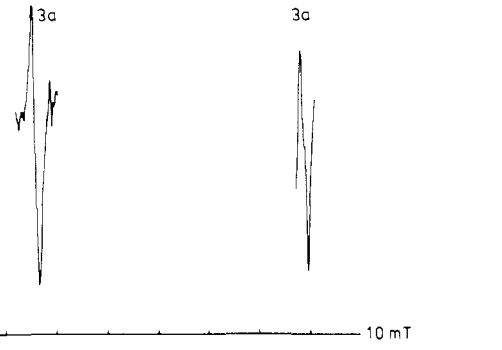

Figure 4. Single-crystal ESR spectrum of radical **3a** at 105 K; magnetic field parallel to *c* axis.

Table III. g and Hyperfine Coupling (MHz) Tensors for **3a**

radical	temp (K)	total tensor		direction cosines *a*	*b*	*c*
3a	105	g	2.004	0.986	0	±0.169
			2.006	0	1	0
			2.008	−0.169	0	±0.986
		^{31}P	1902	0.986	0	±0.169
			1481	0	1	0
			1474	−0.169	0	±0.986
		^{1}H	<17	nearly isotropic		

The ESR spectrum of a X-irradiated single crystal of **3**, recorded at 105 K (Figure 4), exhibits a weak phosphorus doublet which can be attributed to the cyclohexylphosphine sulfide radical anion (**3a**). The low- and high-field transitions are broadened due to additional ^{1}H splitting. Upon rotation of a single crystal in the *ac* plane, two different sites are observed. The spectra of the two sites coalesce for all orientations in which the magnetic field direction is parallel or perpendicular to the *a* or *c* axis. The principal ESR parameters were determined by rotating the crystal in the *ac*, *ab*, and *bc* planes (Table III). The principal hyperfine couplings and *g* values of the two sites are identical within experimental error. The two hyperfine coupling tensors are inclined by an angle of 19.5°, which is close to the crystallographic angle of 15.8° between the two PS bonds. The directions of the ESR parameters of **3a** correspond with the C_s symmetry of the parent molecule. The signals of **3a** are irreversibly lost from the ESR spectrum at temperatures above 160 K.

4. Trimethylphosphine Selenide (4). The crystal structure of trimethylphosphine selenide (**4**) is very similar to that of the corresponding sulfide. The compound crystallizes in the monoclinic space group $P2_1/m$ with unit cell parameters a = 6.453 Å, b = 7.806 Å, c = 6.586 Å, and β = 90.46°.[34] The two molecules in the unit cell lie on a mirror plane with a staggered conformation of the methyl groups. The PSe bond directions of the two molecules are parallel and nearly directed along the crystallographic *a* axis. The deviation is only 1°. Furthermore the crystallographic angle β is close to 90°. This justifies the use of the *a*, *b*, and *c* axes as orthogonal axes for the ESR experiments.

X irradiation of a single crystal of **4**, and analysis of the ESR spectrum at 105 K, reveals the formation of two different phosphorus-centered radicals (Figure 5). The first species, **4a**, exhibits a ^{31}P doublet broadened by ^{1}H splitting. The signals of the second radical product, **4b**, are much weaker and consist of a ^{31}P doublet with an additional splitting of 1.38 mT. Raising the temperature

(34) Cogne, A.; Grand, A.; Laugier, J.; Robert, J. B.; Wiesenfeld, L. *J. Am. Chem. Soc.* **1980**, *102*, 2238.
(35) van Meerssche, M.; Lêonard, A. *Bull. Soc. Chim. Belg.* **1959**, *68*, 683.
(36) Kerr, K. A.; Boorman, P. M.; Misener, B. S.; van Roode, J. G. H. *Can. J. Chem.* **1977**, *55*, 3081.

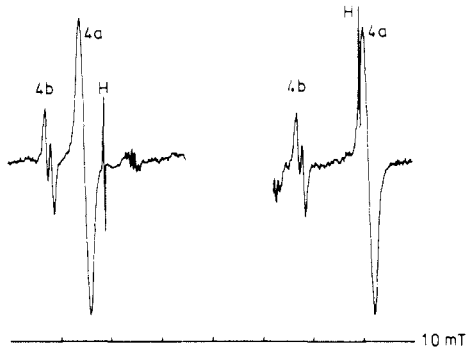

Figure 5. Single-crystal ESR spectrum of **4a** and **4b** at 105 K; magnetic field parallel to the *c* axis.

Table IV. g and Hyperfine Coupling (MHz) Tensors for **4a** and **4b**

radical	temp (K)	total tensor		direction cosines *a*	*b*	*c*
4a	105	g	1.998	1	0	0
			2.003	0	1	0
			2.041	0	0	1
		^{31}P	1937	1	0	0
			1561	0	1	0
			1561	0	0	1
		^{77}Se	783	1	0	0
			193	0	1	0
			200	0	0	1
		^{1}H		not resolved		
4b	105	g	2.001	0.875	0	0.483
			2.072	0	1	0
			2.059	−0.483	0	0.875
		^{31}P	1624	0.854	0	−0.520
			1439	0	1	0
			1408	0.520	0	0.854
		^{1}H	35–40			

shows a decrease of signal intensity for both radicals. At 140 K the small extra coupling of **4b** coalesces into a normal ^{31}P doublet. A further increase of the temperature results in the irreversible loss of **4b** at 180 K and of **4a** at approximately 220 K.

The presence of the ^{77}Se isotope ($I = {}^1/_2$, natural abandance 7.58%) in **4** offers a possibility for the determination of the Se hyperfine interaction in the radicals **4a** and **4b**. The intensity of a single ^{77}Se satellite transition amounts to only 3.79% of the corresponding ^{31}P transition. This weak intensity precluded the analysis of the ^{77}Se satellites for **4b**. For **4a**, however, the ^{77}Se satellites could be clearly identified for most orientations of the single crystal with respect to the magnetic field. The anisotropic ESR spectra reveal that the parallel ^{31}P and ^{77}Se couplings coincide. For perpendicular orientations the ^{77}Se coupling is small and the satellite absorptions lie under the broad ^{31}P transitions. The determination of the perpendicular ^{77}Se couplings was achieved by a regression analysis of A_{Se}^2 versus $\cos^2\theta$.

Rotation of a single crystal of **4** in the crystallographic *ab*, *ac*, and *bc* planes revealed the principal ESR parameters of **4a** and **4b**, and their relative directions (Table IV). For **4a**, the **g** tensor and both ^{31}P and ^{77}Se hyperfine tensors are aligned and directed along the *a* axis and thus along the PSe bond. The two hyperfine tensors possess a near-axial symmetry. These results lead to the conclusion that **4a** has retained the original near C_{3v} symmetry. The **g** and ^{31}P hyperfine tensors do not share the same principal axes for **4b**. The type of symmetry is now C_s, because in the direction of the *b* axis, perpendicular to the *ac* mirror plane, the **g** and ^{31}P tensor have a mutual principal axis. The direction of the maximum anisotropy of **4b** forms an angle of 31° with the PSe bond. The C_s symmetry leads to the suggestion that in **4b** one of the methyl groups contributes more to the SOMO than the other two. The extra splitting of 1.25 mT could then be the result of the trans located CH_3 hydrogen atom in the mirror plane.

5. Triethylphosphine Selenide (5). The crystal structure of triethylphosphine selenide (**5**) is isomorphous with that of the corresponding sulfide (**2**). Triethylphosphine selenide crystallizes

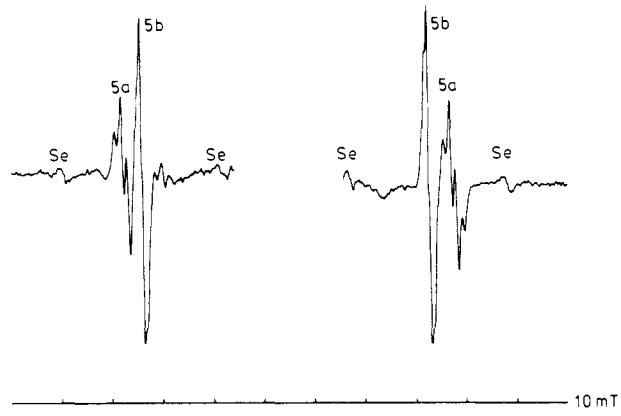

Figure 6. Single-crystal ESR spectrum of **5a** and **5b** at 105 K; magnetic field parallel to *c* axis. The positions of the Se satellites are marked.

Table V. g and Hyperfine Coupling (MHz) Tensors for **5a** and **5b**

radical	temp (K)	total tensor		direction cosines *a*	*b*	*c*
5a	105	g	2.014	1	0	0
			2.014	0	1	0
			1.998	0	0	1
		^{31}P	1399	1	0	0
			1399	0	1	0
			1813	0	0	1
		^{77}Se	268	1	0	0
			268	0	1	0
			862	0	0	1
		^{1}H	33	nearly isotropic		
5b	105	g	2.047	1	0	0
			2.047	0	1	0
			2.003	0	0	1
		^{31}P	1423	1	0	0
			1423	0	1	0
			1579	0	0	1
		^{77}Se	319	1	0	0
			319	0	1	0
			865	0	0	1
		^{1}H	15	nearly isotropic		

in the hexagonal space group $P6_3mc$ with unit cell dimensions $a = 9.06$ Å and $c = 6.54$ Å.[37] All PSe bonds of the molecules in the unit cell are directed along the *c* axis, which is the elongation axis of the needle-shaped crystal.

After X irradiation at 77 K, the ESR spectrum of **5** at 105 K shows the features of two different phosphoranyl radicals **5a** and **5b** (Figure 6). The intensity of the lines attributed to **5b** is appreciably larger than for **5a**. Both radicals exhibit a large ^{31}P hyperfine coupling with an additional splitting from three equivalent ^{1}H nuclei. This extra coupling is somewhat larger for **5a**, and better resolved, than for **5b**. The ^{77}Se satellites are well defined for both species.

As for the corresponding sulfide **2a**, a single-crystal ESR analysis of **5a** and **5b** reveals that both radicals possess axially symmetric **g** and hyperfine tensors (Table V). This must be the consequence of their C_3 symmetry. The parallel features coincide with the PSe bond. The ESR parameters of **5a** and **5b** indicate that their structures are rather similar. Two substantial differences, however, can be noted. First, the value of $\Delta g_\perp$ ($=g_\perp - g_e$) is much larger for **5b** than for **5a**. Second, the difference $A_\parallel - A_\perp$ ($3B$) is for **5b** (156 MHz) significantly smaller than for **5a** (414 MHz). As for **2a** the ^{1}H splitting of **5a** and **5b** results from the trans located CH_2 hydrogen atoms. The signal intensity of **5b** decreases rapidly upon warming, and the radical is irreversibly lost at 205 K. Further warming results in the loss of **5a** at approximately 270 K.

6. Tricyclohexylphosphine Selenide (6). Single crystals of tricyclohexylphosphine selenide (**6**) are colorless well-defined

(37) van Meerssche, M.; Lêonard, A. *Acta Crystallogr.* **1959**, *12*, 1053.

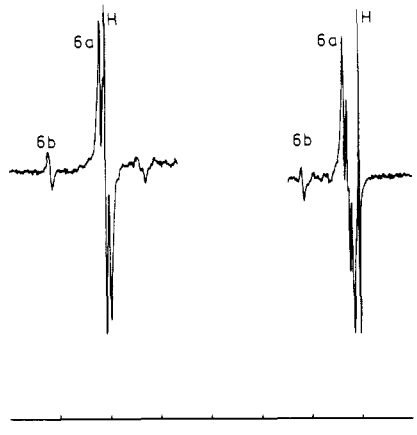

Figure 7. Single-crystal ESR spectrum of **6a** and **6b** at 105 K; magnetic field parallel to z axis.

Table VI. g and Hyperfine Coupling (MHz) Tensors for **6a** and **6b**

radical	temp (K)	total tensor		direction cosines a	b	c
6a	105	g	1.999	0.988	0	±0.156
			2.031	0	1	0
			2.008	−0.156	0	±0.988
		^{31}P	1747	0.988	0	±0.156
			1344	0	1	0
			1332	−0.156	0	±0.988
		^{77}Se	853	~1	0	0
			199	0	1	0
			225	0	0	~1
		^{1}H	28	nearly isotropic		
6b	105	g	2.006	0.987	0	±0.158
			2.072	0	1	0
			2.047	−0.158	0	±0.987
		^{31}P	1562	0.957	0	∓0.289
			1424	0	1	0
			1435	−0.289	0	∓0.957
		^{1}H		not resolved		

plates. No X-ray crystal structure analysis of this compound has been reported.

The ESR spectrum of an X-irradiated single crystal of **6** (Figure 7) shows the features of an electron-capture phosphoranyl radical (**6a**) together with a much weaker spectrum of a second radical product (**6b**). The spectrum of **6a** exhibits additional hyperfine splitting from three ^{1}H nuclei with somewhat different coupling constants. The ^{77}Se satellites of **6a** are well defined for most orientations.

The ESR reference y axis was chosen perpendicular to the plate face, and the x and z axes were chosen, with the use of a polarization microscope, coincident with the extinction directions of the crystal perpendicular to y. When the single crystal is mounted with the y axis parallel to the goniometer axis, a site splitting for **6a** and **6b** is observed. Coalescence of the differently oriented radicals occurs when the magnetic field direction is parallel to x or z. The results of the single-crystal analysis of **6a** and **6b** are compiled in Table VI. The directions of the largest ^{31}P hyperfine coupling for the two orientations of **6a** are inclined by an angle of 18.0°. This result and the fact that the xz plane appears to be a mirror plane leads to the conclusion that the crystals of **6** are isomorphous with tricyclohexylphosphine sulfide (**3**).[36] The ^{77}Se coupling of **6a** was found to be nearly parallel to the ^{31}P coupling. Because of the low intensity of the satellites and the small angle between the two orientations, an accurate determination of the direction cosines was not possible (Table VI).

The analysis of **6b** reveals that its **g** and ^{31}P hyperfine tensors form an angle of 25.9°. The angle between the two ^{31}P tensors of the two orientations is 33.6°, and they are therefore not directed along the PSe bonds. The assignment of the relation between the two orientations of **6a** and **6b** is not without ambiguity. However, based on the C_s symmetry of the parent molecule, the X-ray analysis of the related sulfide **3** and the results of **4a** and **4b**, it

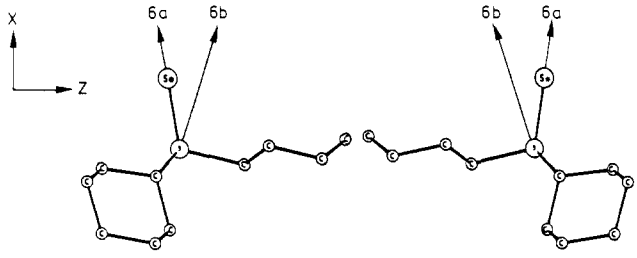

Figure 8. Directions of the principal ^{31}P hyperfine couplings of **6a** and **6b** relative to the x and z axes.

seems likely that the assignment is as shown in Figure 8. From this it follows that from a single molecule of **6** two phosphorus-centered radicals can result with an angle of 25.8° between their principal ^{31}P hyperfine directions. Annealing of the crystal leads to the irreversible loss of **6b** at 140 K and of **6a** at 200 K.

7. Triphenylphosphine Sulfide (7) and Triphenylphosphine Selenide (8). σ^*-Type radicals of triphenylphosphine sulfide (**7**) and triphenylphosphine selenide (**8**) have been reported to be formed in frozen methanolic (**7**)[38] and sulfuric acid (**7**, **8**)[39] solutions. In sulfuric acid the parent phosphine sulfide and selenide are very likely to be protonated, and the formed radicals are probably $Ph_3\dot{P}SH$ and $Ph_3\dot{P}SeH$.

Exposure of powdered samples or single crystals of **7** and **8** to X rays at 77 K does not result in the formation of electron-capture phosphoranyl radicals. The same negative result, regarding phosphoranyl radical formation, was reported by Evans et al. for γ irradiation of pure Ph_3PS.[38]

IV. Quantum Chemical Calculations

In the previous sections it was demonstrated that X irradiation of trialkylphosphine sulfides and selenides at low temperature invariably yields a phosphoranyl radical anion with (approximately) C_3 symmetry. These anions are rather unstable and at temperatures above 200 K their signals irreversibly disappear from the ESR spectra.

Quantum chemical calculations can, in principle, give additional information on the structure of these radicals. It must be borne in mind that, in general, these calculations are performed on a single isolated radical and that effects of surrounding molecules in the single-crystal matrix are neglected. According to Clark, however, ab initio calculations with a restricted basis set can give a good simulation of radical anions in condensed phases.[40,41]

1. Computational Details. The open-shell calculations were performed using several different quantum chemical techniques. Unrestricted Hartree–Fock (UHF) calculations have been carried out using the GAUSSIAN 80 program.[42] The molecular geometries were optimized in an analytical gradient procedure with respect to all parameters within the symmetry constraints. After annihilation of the largest spin contaminant of the UHF wave function, the expectation value of the S^2 operator was always less than 0.7505. Isotropic and anisotropic hyperfine interactions (A_P^{iso} and B_P) were evaluated from the spin-annihilated wave function by computing the expectation values of the corresponding operators.[43] Additionally, hyperfine couplings were computed from the SOMO, neglecting all lower lying α and β MOs. Alternatively, restricted open-shell Hartree–Fock (ROHF) calculations were performed using the GAMESS program package.[44] Configuration interaction (CI) calculations have been carried out using the complete active

(38) Evans, J. C.; Mishra, S. P.; Rowlands, C. C. *Chem. Phys. Lett.* **1980**, *72*, 168.
(39) Eastland, G. W.; Symons, M. C. R. *J. Chem. Soc., Perkin Trans. 2* **1977**, *73*, 833.
(40) Clark, T. *J. Chem. Soc., Chem. Commun.* **1984**, 93.
(41) Clark, T. *Faraday Discuss. Chem. Soc.* **1984**, *78*, 203.
(42) Binkley, J. S.; Whiteside, R. A.; Krishnan, R.; Seeger, R.; DeFrees, D. J.; Schlegel, H. B.; Topiol, S.; Kahn, L. R.; Pople, J. A. GAUSSIAN 80, Department of Chemistry, Carnegie-Mellon University, Pittsburgh, PA.
(43) Janssen, R. A. J.; Buck, H. M. *THEOCHEM* **1984**, *110*, 139.
(44) Guest, M. F. GAMESS, Computational Science Group, SERC Daresbury Laboratory, Daresbury, Warrington. The calculations were performed on the Cyber 205 computer of the Stichting Academisch Rekencentrum Amsterdam.

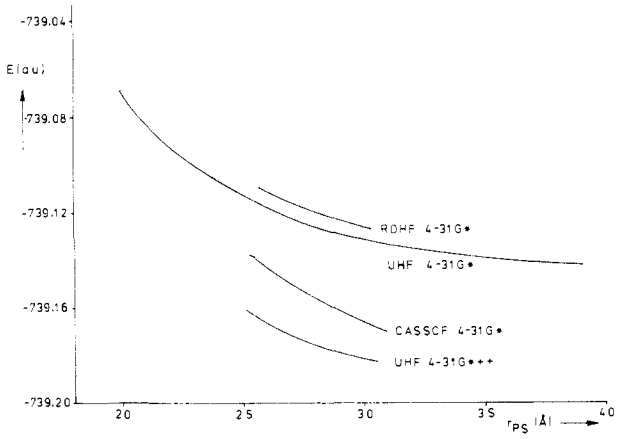

Figure 9. Total energy of $H_3\dot{P}S^-$ within C_{3v} symmetry vs r_{PS} using different computational methods.

space SCF (CASSCF) algorithm of the GAMESS program. In this technique a selection is made of a set of orbitals which are optimized self-consistently and employed in a full CI treatment simultaneously.[45] In all calculations we used a standard 4-31G basis set,[46,47] augmented with a single set of second-order Gaussians on phosphorus and sulfur.[48] In some calculations diffuse orbitals (s and p) were included in the basis set to allow for the accommodation of the negative charge on sulfur.

2. Results of the Calculations. Quantum chemical calculations were performed for $H_3\dot{P}S^-$ as a model for the observed radical anions. Further, we studied the protonated species $H_3\dot{P}SH$, $H_3\dot{P}SH_2^+$, and $H_3\dot{P}SH_3^{2+}$.

a. $H_3\dot{P}S^-$. The UHF calculations predict that within C_{3v} symmetry the three-electron P–S^- bond is unstable and that the radical dissociates into a neutral PH_3 molecule and a $S^{\bullet-}$ radical. At HF/4-31G* level, the sum of the total energies of isolated PH_3 (C_{3v} optimized: PH = 1.406 Å, HPH = 94.1°, E = −341.089 83 au) and $S^{\bullet-}$ (E = −397.052 80 au) lies 1726 kJ mol^{-1} below the alternative electron distribution of $\dot{P}H_3^+$ (C_{3v} optimized: PH = 1.384 Å, HPH = 112.6°, E = −341.775 48 au) and S^{2-} (E = −396.709 59 au). Such a large value for the single-electron transfer energy (ΔE_{SET}) implies a large difference between the energy levels of the HOMO of PH_3 and SOMO of $S^{\bullet-}$, and accounts for the instability of the three-electron bond and its dissociation.

Since the stability of the experimentally observed radical anions may, in principle, be due to matrix interactions preventing dissociation at low temperature, we studied the electronic structure of $H_3\dot{P}S^-$ at fixed PS distances. Figure 9 shows the potential energy curve of C_{3v} $H_3\dot{P}S^-$ as a function of the PS distance (r_{PS}), in which all parameters, except r_{PS}, were fully optimized. The SOMO of the $H_3\dot{P}S^-$ radical anion consists essentially of the phosphorus 3s and the sulfur $3p_z$ orbitals. Upon elongation of the PS bond, the contribution of the sulfur $3p_z$ orbital increases. Simultaneously a decrease of the spin density in the phosphorus 3s orbital and thus of A_P^{iso} (Figure 10) is found. For r_{PS} between 2.4 and 2.5 Å the calculated isotropic hyperfine coupling (1800–1300 MHz) agrees with the experimental values (Table VII). The spin density in the phosphorus $3p_z$ orbital is very small, in contrast with the experimental results. The small phosphorus $3p_z$ spin density is reflected in the calculated values of the dipolar hyperfine interaction ($2B_P$, Figure 11); e.g., at r_{PS} = 2.45 Å the calculated value of $2B_P$ (14 MHz) is only a fraction of the experimental values (100–300 MHz). When the hyperfine couplings are computed from the SOMO, and not from the spin-annihilated wave function, somewhat larger values for A_P^{iso} and $2B_P$ are

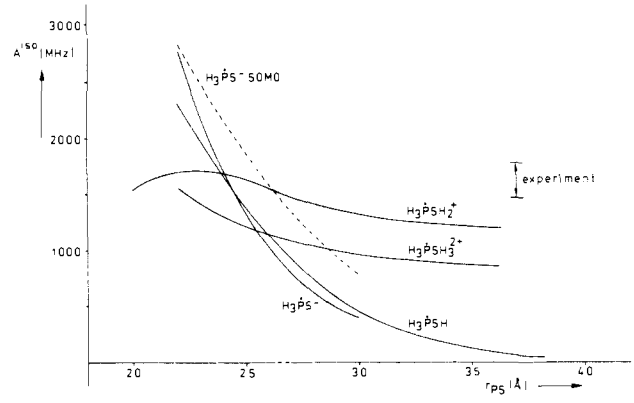

Figure 10. Calculated isotropic phosphorus hyperfine interaction (A_P^{iso}, MHz) vs r_{PS} for $H_3\dot{P}S^-$ (wave function and SOMO), $H_3\dot{P}SH$, $H_3\dot{P}SH_2^+$, and $H_3\dot{P}SH_3^{2+}$.

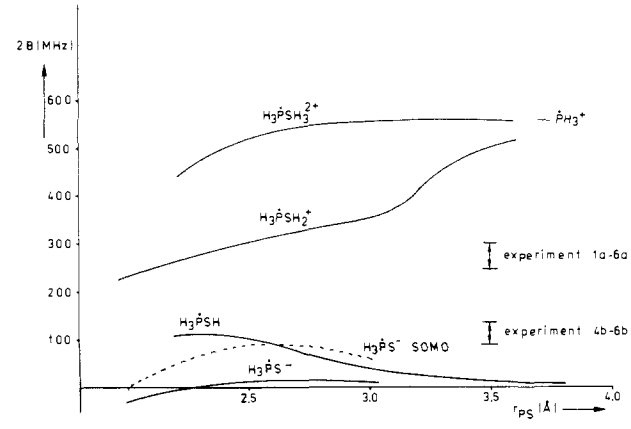

Figure 11. Calculated dipolar phosphorus hyperfine coupling ($2B_P$, MHz) vs r_{PS} for $H_3\dot{P}S^-$ (wave function and SOMO), $H_3\dot{P}SH$, $H_3\dot{P}SH_2^+$, and $H_3\dot{P}SH_3^{2+}$.

predicted; i.e., at r_{PS} = 2.6 Å A_P^{iso} = 1615 MHz and $2B_P$ = 87 MHz. The correspondence with experiment, however, remains unsatisfactory.

In order to improve the description of the nonbonding electron pairs on sulfur two sets of diffuse s and p orbitals (exponents 0.1 and 0.01) were added to the sulfur 4-31G* basis set (4-31G*++). This resulted in a lowering of the total UHF energy by ca. 0.05 au (Figure 9) but caused no substantial improvement of the spin density distribution. A similar result was obtained from CI calculations using the CASSCF routine of the GAMESS program on an ROHF wave function (Figure 9). The employed active space consisted of three doubly, one singly, and three unoccupied MOs resulting in 404 configurations. Despite the energy lowering no significant redistribution of spin density was observed.

Before returning to the H_3PS^- model, it is worthwhile to study the successively protonated species $H_3\dot{P}SH$, $H_3\dot{P}SH_2^+$, and $H_3\dot{P}SH_3^{2+}$. The introduction of one or more protons in the vicintiy of the sulfur nucleus will increase the electronegativity of the sulfur ligand. Because of the antibonding character of the three-electron bond, the increased ligand electronegativity will result in a rise of the unpaired electon density near the phosphorus nucleus:

$$R_3P{:}\ \cdot L \longrightarrow R_3P^{+}\ {:}L^{-}$$

increasing ligand electronegativity

b. $H_3\dot{P}SH$. Recent calculations by Gonbeau et al. show that a tetrahedral configuration of H_3PSH is unstable and results in an immediate elongation of the PS bond, leading to rupture.[49] Our calculations at 4-31G* UHF SCF level confirm this result. Similar to the potential energy curve of $H_3\dot{P}S^-$ we determined the

(45) Larsson, M.; Siegbahn, P. F. M. *J. Chem. Phys.* **1983**, *79*, 2270.
(46) Ditchfield, R.; Hehre, W. J.; Lathan, W. A. *J. Chem. Phys.* **1971**, *54*, 724.
(47) Hehre, W. J.; Lathan, W. A. *J. Chem. Phys.* **1972**, *56*, 5255.
(48) Radial coefficients P = 0.55 and S = 0.65: Francl, M. M.; Pietro, W. J.; Hehre, W. J.; Binkley, J. S.; Gordon, M. S.; DeFrees, D. J.; Pople, J. A. *J. Chem. Phys.* **1982**, *77*, 3654.
(49) Gonbeau, D.; Guimon, M.-F.; Ollivier, J.; Pfister-Guillouzo, G. *J. Am. Chem. Soc.* **1986**, *108*, 4760.

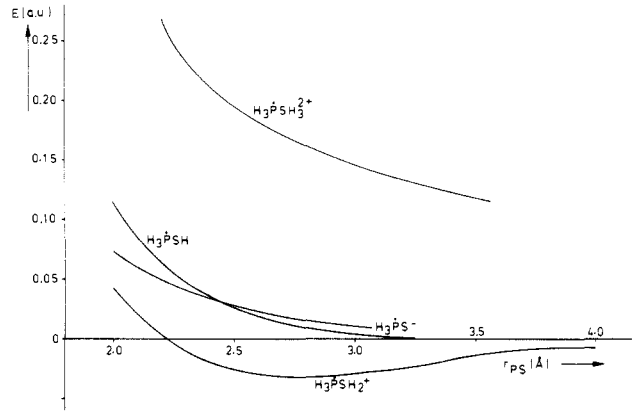

Figure 12. Total UHF energy of $H_3\dot{P}S^-$, $H_3\dot{P}SH$, $H_3\dot{P}SH_2^+$, and $H_3\dot{P}SH_3^{2+}$ vs r_{PS}. The values are relative to the energy of the most favorable dissociation route: $H_3\dot{P}S^-$, −739.142 62 au; $H_3\dot{P}SH$, −739.744 69 au; $H_3\dot{P}SH_2^+$, −740.033 18 au; $H_3\dot{P}SH_3^{2+}$, −740.312 97 au.

total energy of $H_3\dot{P}SH$ as a function of r_{PS} (Figure 12).

In these calculations the H_3P fragment was constrained to a C_{3v} geometry and the sulfur nucleus was positioned in the C_3 axis. The sulfur proton was oriented at a fixed PSH angle of 97°, one HSPH dihedral angle being 180°. All other parameters (PH and SH distance, HPH angle) were fully optimized. By computing the total energy of $\dot{S}H$ ($^2\Pi$ state optimized: SH = 1.331 Å, E = −397.654 86 au) and of SH^- (optimized: SH = 1.349 Å, E = −397.653 47 au), and combining these with the energies of PH_3 and $\dot{P}H_3^+$ (vide supra), a value of ΔE_{SET} = 829 kJ mol^{-1} for $PH_3 + \dot{S}H \rightarrow \dot{P}H_3^+ + SH^-$ is obtained. Although significantly smaller than the corresponding value for $H_3\dot{P}S^-$, this value of ΔE_{SET} is still too large to give rise to a stable three-electron bond. With respect to the spin density distribution, it appears that the isotropic phosphorus hyperfine coupling is approximately equal to that of $H_3\dot{P}S^-$ (Figure 10) but that an increased value for $2B_P$ is calculated. This is the result of an increased phosphorus $3p_z$ unpaired electron population.

c. $H_3\dot{P}SH_2^+$. The addition of a second proton, resulting in $H_3\dot{P}SH_2^+$, leads to the formation of a stable radical geometry containing a three-electron bond. This structure, fully optimized within C_s symmetry, possesses a PS bond length of 2.771 Å. Clark obtained similar structures with PS bond lengths of 2.886 and 2.881 Å at 4-31G SCF and MP2 level, respectively.[11] Our calculations reveal that ΔE_{SET} for $PH_3 + \dot{S}H_2^+ \rightarrow \dot{P}H_3^+ + SH_2$ amounts only −53.6 kJ mol^{-1}, i.e., near to thermoneutral (total energies: $\dot{S}H_2^+$ C_{2v} $^2B_1$ state optimized SH = 1.335 Å, HSH = 95.4°, E = −397.992 93 au; SH_2 C_{2v} optimized SH = 1.326 Å, HSH = 93.8°, E = −398.257 69 au; PH_3 and $\dot{P}H_3^+$, vide supra). This results in a stable three-electron bond and a dissociation energy of 79.3 kJ mol^{-1} with respect to $\dot{P}H_3^+$ and SH_2. The potential energy curve of $H_3\dot{P}SH_2^+$ vs. r_{PS} is shown in Figure 12. All molecular parameters were fully optimized within C_s symmetry constraint. At the geometry of minimal energy, but also for other values of r_{PS} between 2.2 and 3.0 Å, the calculated values of A_P^{iso} and $2B_P$ are close to the experimental couplings of the trialkylphosphine sulfide radical anions (Table VII). E.g., at r_{PS} = 2.771 Å, A_P^{iso} = 1438 MHz and $2B_P$ = 327 MHz. This result clearly demonstrates that a rise of the electronegativity of the sulfur ligand results in an increased spin density at phosphorus. Because of the C_s symmetry of the optimized structure and the relatively large H_1PS angle of 143.1°, the direction of the phosphorus dipolar hyperfine coupling makes an angle of 31.3° with the PS bond.

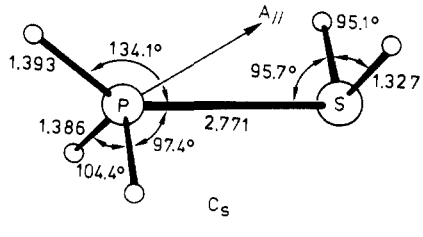

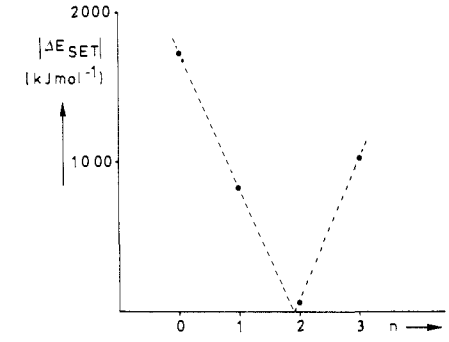

Figure 13. Single-electron transfer energy (ΔE_{SET}) for $PH_3 + \dot{S}H_n^{n-1} \rightarrow \dot{P}H_3^+ + SH_n^{n-2}$ vs the number of protons n.

d. $H_3\dot{P}SH_3^{2+}$. The potential energy curve of C_{3v} $H_3\dot{P}SH_3^{2+}$ (Figure 12) reveals a rapid dissociation of the PS bond, in agreement with the large calculated value of ΔE_{SET} = −1026 kJ mol^{-1} for $PH_3 + \dot{S}H_3^{2+} \rightarrow \dot{P}H_3^+ + SH_3^+$ which is obtained from the total energies of PH_3 and PH_3^+ (vide supra) and those of $\dot{S}H_3^{2+}$ (C_{3v} optimized: SH = 1.373 Å, HSH = 117.7°, E = −397.832 21 au) and SH_3^+ (C_{3v} optimized: SH = 1.331 Å, HSH = 96.6°, E = −398.537 49 au). During the dissociation, the electronic structure of the complex is essentially equal to that of an isolated $\dot{P}H_3^+$ radical, with a minor contribution from the sulfur orbitals.

From these calculations it appears that a stable three-electron bond is formed when the absolute value of ΔE_{SET} is small (Figure 13), i.e., for the $H_3\dot{P}SH_2^+$ radical cation. Unfortunately, no experimental analogue of this radical has been reported. In contrast, for the $R_3\dot{P}S^-$ radical anions presented in this paper, and for the $(CH_3)_3\dot{P}SH$ and $(CH_3)_3\dot{P}SCH_3$ radicals which are formed in liquid cyclopropane at 170 K,[50] the model calculations predict a rapid elongation of the bond resulting in rupture.

e. $H_3\dot{P}S^-$ in the Presence of Additional Charges. It is clear that the present calculations do not give an adequate simulation of the electronic structure and stability of $R_3\dot{P}S^-$ and $R_3\dot{P}SR$ radicals in condensed phases. A major drawback of the calculations seems to be the rather poor description of the nonbonding electron pairs on sulfur. For this reason we studied the spin density distribution and electronic structure of $H_3\dot{P}S^-$ in the presence of additional point charges. In our ROHF calculations the sulfur 4-31G* basis set was augmented with a single set of diffuse s and p orbitals (exponent 0.1). The $H_3\dot{P}S^-$ radical was placed between a positive and negative point charge of the same absolute magnitude in the following fixed C_{3v} orientation:

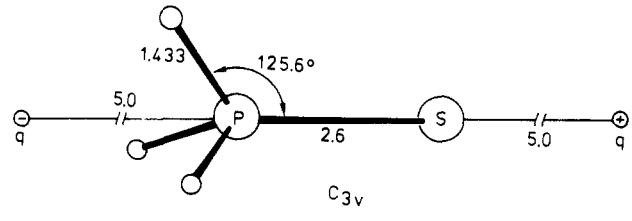

From the calculated atomic spin density on sulfur and phosphorus as function of the charge q (Figure 14), it appears that with increasing charge the unpaired electron shifts to the phosphorus nucleus. This is the result of the electron-withdrawing positive charge near sulfur, which induces a delocalization of the nonbonding electrons to the outer valence and diffuse orbitals. From Figure 14 it is clear that by an adequate placement of external charges the calculated spin density can be modulated to a range of spin density distributions between phosphorus and sulfur. For q between 3 and 4 au the theoretical spin density distribution is in accordance with the experimental data. The improved correspondence between theory and experiment obtained via the introduction of point charges demonstrates some limitations of ab initio theory when applied to isolated radical anions as

(50) Giles, J. R. M.; Roberts, B. P. *J. Chem. Soc., Perkin Trans. 2* **1981**, 1211.

Table VII. Isotropic and Dipolar Hyperfine Couplings (MHz) and Approximate Orbital Spin Densities (%)

	^{31}P				^{77}Se				^{1}H	
radical	A^{iso}	$2B$	ρ_s	ρ_p	A^{iso}	$2B$	ρ_s	ρ_p	A^{iso}	ρ_s
1a	1776	245	13.3	33.3					13	0.9
1b	±917	∓145	±6.9[a]	∓19.8[a]					13	0.9
2a	1659	284	12.5	38.7					34	2.4
3a	1619	283	12.2	38.6					<17	1.2
4a	1686	251	12.7	34.2	392	391	1.9	39.8		
4b	1490	134	11.2	18.3					35	2.5
5a	1537	276	11.6	37.6	466	396	2.3	40.2	38	2.7
5b	1475	104	11.1	14.2	501	364	2.5	37.0	15	1.1
6a	1474	300	11.1	40.9	426	427	2.1	43.4	28	2.0
6b	1474	88	11.1	12.0						

[a] Calculated for valence orbital couplings (see text).

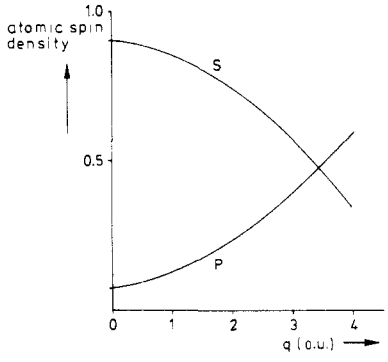

Figure 14. Atomic spin density on phosphorus and sulfur vs the charge q.

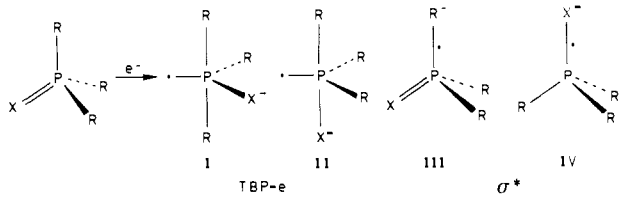

Figure 15. Possible TBP-e and σ^* structures for $R_3\dot{P}S^-$ radicals.

prototype systems for trapped radicals in the solid state.

V. Discussion

Phosphoranyl radicals generated by radiation-induced electron capture of four-coordinated phosphorus compounds ($R_3P{=}X$) can, in principle, adopt several different structures. Two frequently observed structures are a trigonal-bipyramidal configuration with the unpaired electron in an equatorial position (TBP-e)[51] and a tetrahedral σ^* structure containing a three-electron bond.[23] Depending on the topology of the distribution of the substituents, two different TBP-e and two σ^* configurations can result (Figure 15).

The formation of one of these structures, or an intermediate configuration, depends on the nature of the substituents R and X. If the substituents R are not identical, the number of possible configurations increases and the relative site preference of the substituents R is important.[52] Structures of type I to III have been identified and investigated by single-crystal ESR.[53,54] The present study on trialkylphosphine sulfide and selenide radical anions gives the first single-crystal ESR evidence of type IV configurations. Table VII comprises the isotropic and anisotropic hyperfine couplings for the studied radicals together with the approximate orbital spin densities.[55] Radicals **1a**, **2a**, **3a**, **4a**, **5a**, and **6a** clearly possess a similar spin density distribution. The phosphorus 3s contribution lies in the range of 11 to 14%, and 33 to 41% is located in the 3p orbital. The unpaired electron density on selenium is approximately 40%, mainly confined to the 4p orbital. All radicals show a small spin delocalization on the α hydrogen nuclei of the alkyl groups. The isotropic ^{31}P hyperfine coupling decreases in the series methyl > ethyl > cyclohexyl, and is consequently larger for the sulfide than for the corresponding selenide. The dipolar hyperfine coupling for the methyl derivatives (**1a**, **4a**) is smaller than those of the ethyl- and cyclohexyl-substituted compounds (**2a**, **3a**, **5a**, **6a**). The ^{31}P and ^{77}Se anisotropic hyperfine couplings are directed along the PS or PSe bonds of the precursor molecules. The p/s ratio for ^{31}P varies from 2.5 to 3.7.

There is no doubt that radicals **1a**–**6a** are indeed anionic and maintain the structural integrity of their precursors. The SOMO of a radical cation generated from R_3PX molecules would be a nonbonding valence p(π) orbital on sulfur or selenium, and the delocalization onto phosphorus is consequently very small since it arises from spin polarization or via suitable 3d orbitals, resulting in a low A_P^{iso}.[56] Moreover, a positive g_{zz} shift would be expected. Alternatively, a possible rupture of the P–X bond is in contrast with the observed hyperfine coupling to both phosphorus and selenium. Finally, a dissociation of a P–R bond would generate a phosphonyl-type radical ($R_2\dot{P}X$), which is well described and possesses a substantially lower A_P^{iso} value.[4,57,58] Furthermore, a P–R bond dissociation would certainly result in a large deviation from C_3 symmetry, and the principal hyperfine couplings would not be found parallel to the original P–X bonds.

All the structural data lead to the conclusion that the radicals possess a three-electron PS or PSe bond in which the unpaired electron is located in an axial symmetric antibonding σ^* orbital.

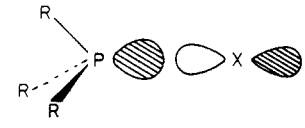

It is noteworthy that upon annealing no dissocation from the $R_3\dot{P}S^-$ and $R_3\dot{P}Se^-$ σ^* radicals into $R_3\dot{P}^+$ radical cations is observed, since rupture of a three-electron bond has been established for other σ^* radicals.[54] The trigonal symmetry of the $R_3\dot{P}X^-$ radicals differs from the results of Geoffroy et al. on chalcogeno triphenylarsoranyl radicals ($Ph_3\dot{A}sX^-$, X = O, S, Se).[59] A detailed study of these species, trapped in single crystals, has shown that the maximum ^{75}As coupling forms an angle of 20° with the parent As=S bond, indicating a deviation from C_3 symmetry.

Since the spin densities of **1a**–**3a** and **4a**–**6a** are not very sensitive to the nature of the irradiated compound, it can be concluded that a matrix effect is not an important factor for the structure of these

(51) Hasegawa, A.; Ohnishi, K.; Sogabe, K.; Miura, M. *Mol. Phys.* **1975**, *30*, 1367.
(52) Janssen, R. A. J.; Buck, H. M. *Chem. Phys. Lett.* **1986**, *132*, 459.
(53) Gillbro, T.; Williams, F. *J. Am. Chem. Soc.* **1974**, *96*, 5032.
(54) Janssen, R. A. J.; Sonnemans, M. H. W.; Buck, H. M. *J. Am. Chem. Soc.* **1986**, *108*, 6145.
(55) Morton, J. R.; Preston, K. F. *J. Magn. Reson.* **1978**, *30*, 577.
(56) Symons, M. C. R.; Janes, R. *J. Chem. Soc., Faraday Trans. 1* **1987**, *83*, 383.
(57) Geoffroy, M. *Helv. Chim. Acta* **1973**, *56*, 1553.
(58) Ayant, Y.; Thevaud, A.; Werbelow, L.; Tordo, P. *J. Magn. Reson.* **1987**, *72*, 251.
(59) Geoffroy, M.; Llinares, A.; Krzywanska, E. *J. Magn. Reson.* **1984**, *58*, 389.

radicals. Nevertheless, the principal hyperfine couplings and g values reflect, in an elegant way, the symmetry properties of the precursor crystal structures. The complete axial symmetry of the **A** and **g** tensors of the radicals **2a** and **5a** is a result of the hexagonal space group of the crystals of **2** and **5**. The radicals **1a**, **3a**, **4a**, and **6a** originate from the molecules of C_s symmetry. Although the deviation of the geometry of **4** from C_{3v} toward C_s symmetry is very small and the corresponding phosphoranyl radical **4a** possesses a principal axis along the PSe bond (near C_3 axis), a very large difference is found for the two perpendicular g values. This must be the result of steric and electronic constraints imposed upon the radical by the surrounding crystal matrix. Similar effects are found for the radicals **1a**, **3a**, and **6a**.

Until now no satisfying assignment can be made to the nature of radical **1b**. This radical seems to be formed from **1a** upon warming and is relatively stable. The single-crystal analysis and powder spectrum of **1b** (Figure 2c) clearly indicate an opposite sign for A^{iso} and B. Because of the relatively large value of the hyperfine coupling, **1b** must be a phosphorus-centered radical. Furthermore, the presence of additional ^1H splitting and the fact that the principal axes of the **A** and **g** tensor are parallel to the PS bond of the precursor molecule lead to the suggestion that the three methyl groups remain covalently bonded to the central phosphorus atom. It is unlikely that **1b** is a trimethylphosphonium radical cation, since the $(CH_3)_3\dot{P}^+$ radical is known to possess approximately 10% 3s and over 90% 3p character.[7,60] The absolute values of A_P^{iso} and B_P of **1b** are too large to be the result of spin polarization. The reason for a negative value of A_P^{iso} or $2B_P$ remains unclear since there is no obvious explanation to justify extensive inner-shell polarization or a large contribution of a phosphorus $d_{x^2} + d_{y^2}$ orbital combination (which could yield a negative value for B_{zz}[61]) to the SOMO.

Irradiation of trialkylphosphine selenides generated besides the σ^* structure (**4a**, **5a**, **6a**) a second species (**4b**, **5b**, **6b**). The thermal stability of these second radical species is much less than the stability of the first, and they are quickly lost upon slight annealing. The isotropic phosphorus hyperfine coupling of **4b–6b** is somewhat smaller than for **4a–6a**. The most striking difference, however, is the low magnitude of the anisotropic hyperfine coupling ($2B_P$, Table VII) and the large deviation of $g_\perp$ from the free-electron value. Radicals **4b**, **5b**, and **6b** are tentatively assigned to σ^*-like structures, although it is not yet fully understood why the SOMO of these species possess a small phosphorus $3p_z$ contribution. As mentioned in sections III.4 and III.6, radicals **4b** and **6b** show a considerable distortion from C_3 symmetry toward C_s, because the direction of $2B_P$ and the parent P=Se bond form an angle of 31 and 26°, respectively. This indicates that **4b** and **6b** possess an intermediate structure between a σ^* and TBP-e configuration. The formation of only one orientation of **4b** in a crystal of **4**, of at least three possibilities, again emphasizes the subtle effects of matrix interactions. In contrast to **4b** and **6b**, **5b** possesses an exact C_3 symmetry and can therefore not possess some TBP-e character. In principle, **5b** could possess a apical position (TBP-a).[62,63] However, the large spin density on selenium (Table VII) argues against this possibility and favors a σ^* configuration. The orbital population of **5a** and **5b** indicate a nearly equal contribution of the selenium $4p_z$ orbitals to the SOMO. The large positive value of $\Delta g_\perp$ for **5b** with respect to **5a** must therefore originate from a relatively nearby filled e orbital which contains large contributions of the selenium $4p_x$ and $4p_y$ orbitals.[64]

The quantum chemical calculations on an isolated $H_3\dot{P}S^-$ radical have clearly shown that the three-electron P–S bond is unstable and dissociates into H_3P and $S^{\bullet-}$. Even at fixed PS distances the theoretical calculations do not reproduce the observed spin density distribution, but tend to localize the unpaired electron entirely on sulfur. It seems questionable that the large differences between computed and observed spin density distribution may be accounted for by the specific conditions inherent in matrix experiments because the nature of the irradiated compound does not seriously affect the exprimental couplings. The origin of the deficiency of the theoretical calculations is predominantly due to a poor description of the negative charge on the sulfur atom, i.e., an inadequate description of the sulfur nonbonding electron pairs. This was demonstrated by introducing a positive point charge in the vicinity of the sulfur atom. In this way the theoretical spin density can be brought into accordance with the experimental data. Alternatively, the radical can be protonated ($H_3\dot{P}SH_2^+$) resulting in a stable three-electron bond and an accurate description of experimental hyperfine couplings. The important effect of the positive charge is to shield the nonbonding electrons and cause a shift of unpaired electron density toward phosphorus.

In view of these results it appears that extreme caution must be used in employing theoretical calculations on isolated radical anions for the simulation of trapped radicals in condensed phases.

Acknowledgment. This investigation has been supported by the Netherlands Foundation of Chemical Research (SON) with financial aid from the Netherlands Organization for the Advancement of Pure Research (ZWO). We thank Mr. G. C. Groenenboom and Mr. M. J. van der Woerd for their assistance in the quantum chemical calculations.

Registry No. **1**, 2404-55-9; **1a**, 112613-48-6; **2**, 597-51-3; **2a**, 113379-52-5; **3**, 42201-98-9; **3a**, 113379-53-6; **4**, 20819-54-9; **4a**, 113379-54-7; **5**, 21522-01-0; **5a**, 113403-27-3; **6**, 52784-98-2; **6a**, 113379-55-8; **7**, 3878-45-3; **8**, 3878-44-2; $H_3\dot{P}S^-$, 113403-12-6; $H_3\dot{P}SH$, 102780-10-9; $H_3\dot{P}SH_2^+$, 87141-20-6; $H_3\dot{P}SH_3^{2+}$, 113379-56-9.

(60) Symons, M. C. R.; McConnachie, G. D. G. *J. Chem. Soc., Chem. Commun.* **1982**, 51.
(61) Weltner, W. *Magnetic Atoms and Molecules*; Scientific and Academic Editions: New York, 1983.
(62) Hamerlinck, J. H. H.; Schipper, P.; Buck, H. M. *J. Am. Chem. Soc.* **1980**, *102*, 5679.
(63) Janssen, R. A. J.; Visser, G. J.; Buck, H. M. *J. Am. Chem. Soc.* **1984**, *106*, 3429.

(64) The g shift arises from the admixture of excited states with the ground state of the radical. The positive value of $\Delta g_\perp$ for the C_{3v} radicals indicates that the induced mixing of the ground state $|0\rangle$ with an excited state $|n\rangle$ involves a transfer of one of the paired electrons of a filled e orbital into a half-filled a_1 orbital. Using only the valence orbitals of phosphorus and selenium, the value $\Delta g_\perp$ can be obtained from first-order perturbation theory (Atkins, P. W.; Symons, M. C. R. *The Structure of Inorganic Radicals*: Elsevier: Amsterdam, 1967):

$$\Delta g_\perp = \{2[c_{3p_z}(P)c_{3p_y}(P) + c_{4p_z}(Se)c_{4p_y}(Se)] \times [c_{3p_z}(P)c_{3p_y}(P)\zeta_P + c_{4p_z}(Se)c_{4p_y}(Se)\zeta_{Se}]\}/(E_n - E_0)$$

where $E_n - E_0$ is the (positive) energy difference between the two states and ζ_P (=299 cm^{-1}) and ζ_{Se} (=1688 cm^{-1}) are the spin–orbit coupling contants. The orbital populations of the SOMO of **5a** and **5b** indicate that $c_{4p_z}(Se)$ is approximately equal for both radicals and that $c_{3p_z}(P)$ is smaller for **5b** than for **5a**. The large value of $\Delta g_\perp$ for **5b** must therefore originate from an increase of $c_{4p_x}(Se)$ and $c_{4p_y}(Se)$ or a decrease of $E_n - E_0$.